Series-Input Parallel-Output Modular-Phase DC–DC Converter With Soft-Switching and High-Frequency Isolation

Ali Mohammadpour, Leila Parsa, Maja Harfman Todorovic, Rixin Lai, Rajib Datta, and Luis Garces

***Abstract*—Multiphase soft-switching high-frequency isolated dc–dc converter is proposed for power conversion in modular stacked HVDC power transmission and distribution system. Input-series output-parallel connection of current-fed full-bridge dc–dc converter modules is proposed to increase voltage blocking capability at the input and decrease current ripple at the output. Basic power electronic building block is zero-current switching (ZCS) full-bridge phase-shift pulsewidth-modulated (PWM) dc–dc converter. Phase shift between switches in each leg of the converter is adjusted to control power flow, while phase shift between gate signals of individual phases is selected according to the number of phases in order to minimize ripple of the output voltage. Converter analysis is carried out to develop a simple equivalent boost converter model of the three-phase soft-switching converter suitable for system-level analysis and simulation. Strategies are developed to ensure fast detection of faults and continued operation of the converter in the case of fault in one phase module. To verify the proposed system design and analysis, experimental results on scaled-down laboratory prototype are presented for a three-phase ZCS dc–dc converter.**

***Index Terms*—Isolated dc–dc converter, subsea power distribution, zero-current switching (ZCS).**

I. Introduction

RECENTLY, high-frequency isolated dc–dc power conversion has gained special interest in high power applications, including renewable energy power conversion, power distribution in microgrids, and solid-state transformers [1]–[4]. Modular design of high-frequency isolated dc–dc power conversion provides high reliability and high power density as two essential requirements of such applications [5]–[16].

Design of power transmission and distribution system for distant subsea oil and gas fields is an emerging research area with complex technical challenges. The oil and gas industry is searching for more efficient approach for power delivery to subsea loads that offers high reliability and high power density without significant increase in overall system cost. This growing interest is primarily caused by recent electrification trends in oil and gas industry that demand electric power for subsea systems, including pumps and compressors, electronic control and communication systems, etc. The power transmission and distribution level is in the range of tens of MWs to be distributed to loads located as low as few miles in the sea bed. Electric loads are usually distributed at subsea locations over a short or long distance. In addition electric loads for newly discovered reserves need to be connected to established power system [17]–[22].

For subsea oil and gas fields where bulk power is transmitted over long distance, ac transmission provides technical challenges. The problem gets more severe for high-power loads distributed over long distances. Additional charging current flows along the length of submarine ac cable due to capacitance of the cable. This capacitive charging current reduces the capability of the cable for carrying useful load current. Longer cable lengths result in higher capacitance and higher charging current since capacitance is distributed along the length of the cable.

For long distance, dc transmission has shown to be more efficient compared to ac transmission. Power electronic converters are required to connect HVDC and HVAC systems. Recent advances in high-voltage semiconductor device technology have enabled power electronics technology to penetrate in power transmission and distribution (T&D) systems using insulated gate bipolar transistor (IGBT) and integrated gate commutated thyristors (IGCTs). Conventionally, switches of the converter are designed to handle voltages in the ranges of tens of kilovolts to hundreds of kilovolts. For this purpose, switches are arranged with series connection of several IGBTs or thyristors. Large size and high count of component limit application of conventional HVDC systems in subsea power systems. A promising system topology for subsea power T&D, modular stacked direct current (MSDC) is presented in [23]. The system is composed of cascade symmetrical connection of modular three-level converters in sending end and receiving end of the T&D system. The transmission line current is adjusted by a control loop to follow command value that depends on the subsea load power. Robust, modular, and fault-tolerant design of the systems makes it a top candidate for subsea field power system. However, a major shortcoming of systems is caused by bulky low-frequency subsea transformers resulting in increased volume and mass of the system as well as reduced reliability/maintainability. Objective of this paper is to study replacement of dc–dc converters in the receiving end of

Manuscript received March 19, 2014; revised May 14, 2014 and July 31, 2014; accepted November 13, 2014. Date of publication February 3, 2015; date of current version September 21, 2015. This paper was presented in part at the IEEE Industrial Electronics Conference 2013. Recommended for publication by Associate Editor H.-P. Nee.

A. Mohammadpour is with Bose Corporation in Framingham, MA 01701 USA (e-mail: ali.mdpour@gmail.com).

L. Parsa is with the Department of Electrical, Computer, and Systems Engineering, Jonsson Engineering Center, Rensselaer Polytechnic Institute, Troy, NY 12180 USA (e-mail: parsa@ecse.rpi.edu).

M. H. Todorovic, R. Lai, R. Datta, and L. Garces are with the GE Global Research, Niskayuna, NY 12309 USA (e-mail: harfmanm@ge.com; Lai@ge.com; Rajib.Datta@ge.com; garces@ge.com).

Color versions of one or more of the figures in this paper are available online at http://ieeexplore.ieee.org.

Digital Object Identifier 10.1109/TPEL.2015.2398813

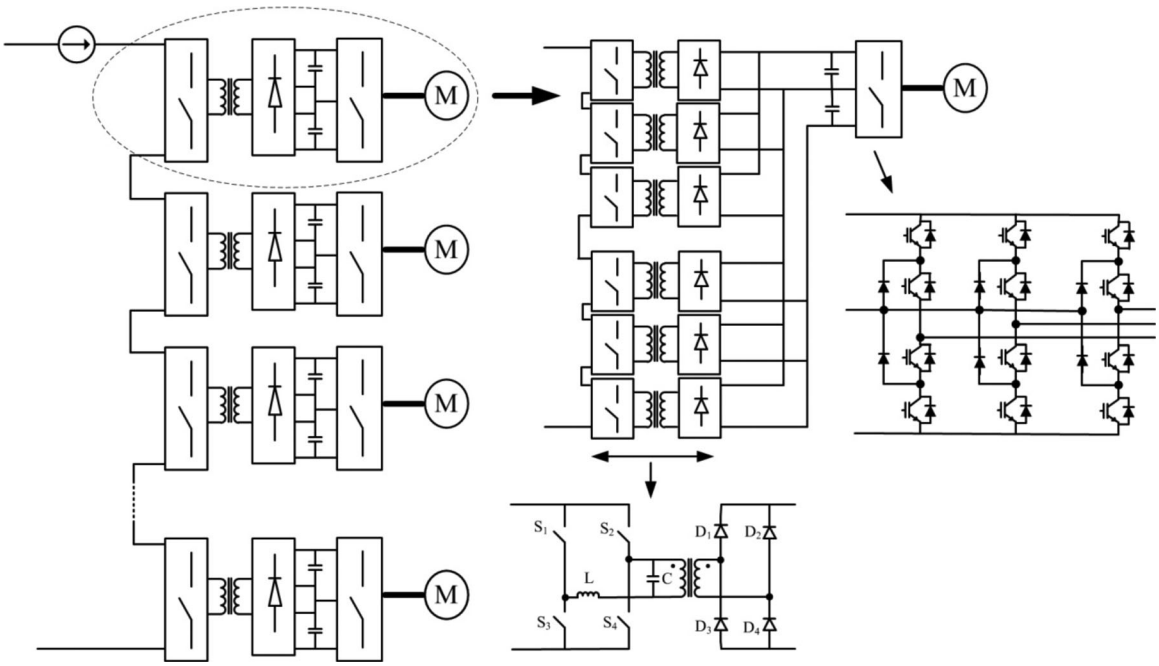

Fig. 1. Schematic view of the proposed power conversion system with a three-phase inverter.

the system with high-frequency isolated dc–dc converters. Mohammadpour *et al*. [24] have proposed high-frequency isolated modular system architecture where preliminary open-loop operation results were presented. In this paper, detailed analysis of converter operation, small-signal modeling, closed-loop control loop design, fault detection, and fault-tolerant operation of the converter are discussed with comprehensive experimental test results. Selection of the basic converter topology is limited by several application dependent requirements such as current-fed input, voltage and power level, and high-frequency galvanic isolation. Here, current-fed phase-shift full-bridge converter is utilized as the basic building block [25]. This converter is dual of well-known voltage-fed zero-voltage-switching (ZVS) phase-shift PWM dc–dc converter. The current-fed converter offers ZCS for all primary IGBTs and ZVS for secondary diodes.

This paper is organized as follows. Proposed architecture for subsea power distribution is presented in Section II. Steady-state analysis and modeling of proposed multiphase ZCS current-fed dc–dc converter is discussed in Section III. Small-signal modeling and control of the converter is discussed in Section IV. Experimental test results on scaled-down laboratory prototype are presented in Section V. Finally, Section VI concludes the paper.

II. Subsea Power System Architecture

Schematic view of the proposed MSDC-based subsea power distribution system is illustrated in Fig. 1. Proposed power conversion system is based on high-frequency isolated two-level dc–dc converters with series connected inputs and parallel connected outputs. Three-level inverters are used at the output of power conversion system to offer speed and torque control for ac motors. Input ports of the converter modules are connected in series. Outputs of the modular converters are connected in a parallel-series configuration to provide a three-level dc link for three-level inverters. The decision for the number of modules connected in parallel or series is based on the voltage and current rating of the transmission line and dc link of the load. Interleaving is utilized to reduce current and voltage ripple at the intermediate dc link. Input stage modules are current-fed zero-current-switching full-bridge PWM boost converters with switching frequency in the range of tens of kilohertz. For isolated boost converter, phase shift between two adjacent switches of the two legs is controlled to regulate the output voltage. Furthermore, primary switches need to have reverse voltage blocking capability. Galvanic isolation of dc–dc converters at the input stage of subsea power conversion system creates flexibility in design and interconnection of output stage. Fig. 2 shows detailed schematic view of a three-phase version of the proposed dc–dc power converter. Steady-state analysis and dynamic modeling of the three-phase converter as well as its fault-tolerant control will be discussed in the following sections.

III. Steady-State Modeling and Analysis

Schematic view of a three-phase version of the proposed dc–dc power converter is shown in Fig. 2. Each phase module is a full-bridge zero-current switching dc–dc converter. Reverse voltage blocking capability is required for primary full-bridge switches. Fig. 3 displays steady-state waveforms of one phase module. Upper leg switches, i.e., S_{1A} and S_{1B}, have complementary gate signals with a small overlap that is utilized for ZCS. On the other hand, in order to control power flow in the converter, gate signals for lower leg switches, i.e., S_{2A} and S_{2B}, are phase-shifted with respect to gate signals of upper leg.

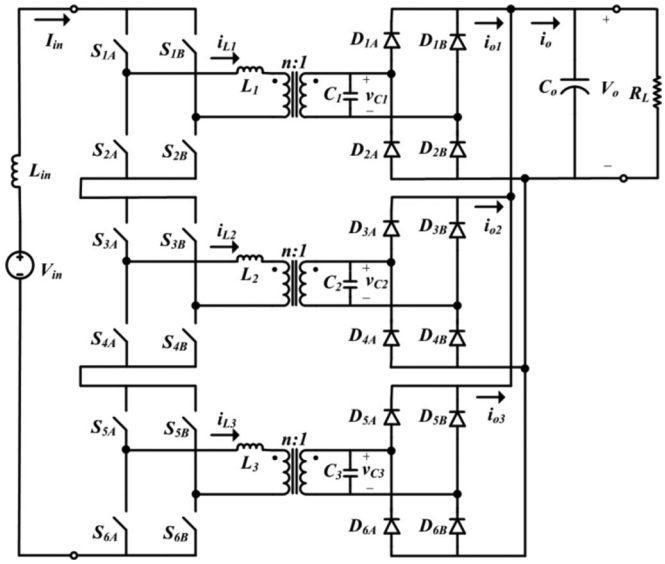

Fig. 2. Three-phase ZCS dc–dc converter.

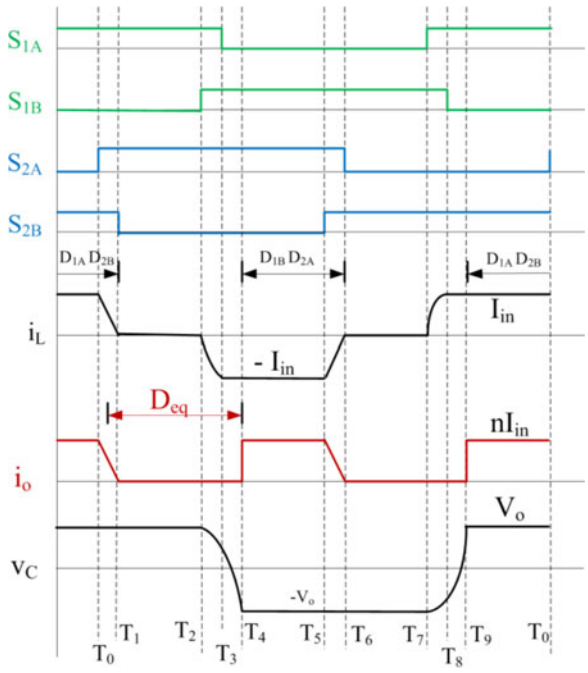

Fig. 3. Waveforms of one module of the proposed three-phase converter.

Here, steady-state converter operation is analyzed to develop a simple model that is suitable for system-level simulation while it takes into account the effect of ZCS. Resonant frequency ω_o and characteristic impedance Z_o of *LC* circuit formed by leakage inductance of transformer and auxiliary secondary capacitor are defined as

$$\omega_o = \frac{1}{\sqrt{LC}}, \qquad Z_o = \sqrt{\frac{L}{C}} \tag{1}$$

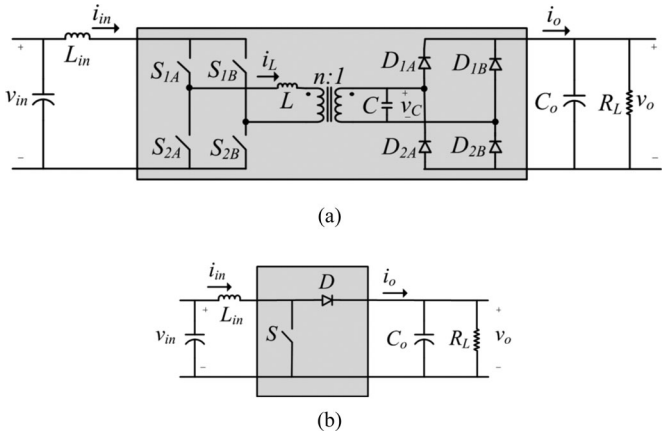

Fig. 4. (a) Phase-shift full-bridge ZCS converter and (b) basic boost equivalent.

where L and C are inductor and capacitor of the resonant circuit, respectively. Normalized input current $J_{\rm in}$ is defined as

$$J_{\rm in} = \frac{Z_o I_{\rm in}}{V_o} \tag{2}$$

where $I_{\rm in}$ is the input current and V_o is the output voltage. In order to calculate the length of each interval in terms of normalized input current and resonant circuit parameters, interval-by-interval analysis of the converter is carried out. The length of the first, third, and fourth intervals are calculated using circuit analysis within that interval. The second interval duration is the control parameter that is set by phase shift of gate signals. Finally, duration of the last interval is easily found by taking into account constant switching frequency of the converter. As it can be seen from Fig. 3, the converter is operating in the second and last intervals for most portion of switching period. These two intervals are equivalent to on state and off state of a basic boost converter. Therefore, based on this analogy, ZCS converter can be analyzed similar to a basic hard-switching boost converter. Table I summarizes all the equations of the converter for steady-state operation. Conducting devices are given during each interval. Equations are presented for leakage inductor current and resonant capacitor voltage. Length of the first, third, and fourth intervals are given as a function of normalized input current. As mentioned earlier, the other two intervals are specified by phase shift and switching frequency of the converter. Fig. 4 shows one module of interleaved converter and its basic boost equivalent. Investigation of this model and converter waveforms suggest the following formula for duty cycle of equivalent basic boost:

$$D_{\rm eq} = \frac{T_{01} + 2\left(T_{12} + T_{23} + T_{34}\right)}{T_s} \tag{3}$$

where

$$T_{ij} = T_j - T_i, \qquad i = 0, 1, 2, 3, \text{ and } j = i + 1 \tag{4}$$

where T_j is switching instant shown in Fig. 3. The output current waveform is almost square wave if small overlap duration is not considered. Duty cycle of the square waveform is

TABLE I
SUMMARY OF EQUATIONS DESCRIBING STEADY-STATE OPERATION OF THE CONVERTER

Mode	Conducting Devices	$i_L(t)$	$v_C(t)$	$\omega_o T_{ij}$
$I:[T_0-T_1]$	$S_{1A}, S_{2A}, S_{2B}, D_{1A}, D_{2B}$	$\frac{-V_o}{L}(t-t_0)+I_{\rm in}$	V_o	$J_{\rm in}$
$II:[T_1-T_2]$	S_{1A}, S_{2A}	0	V_o	–
$III:[T_2-T_3]$	S_{1A}, S_{1B}, S_{2A}	$\frac{-V_o}{Z_o}\sin(\omega_o(t-t_0))$	$V_o\cos(\omega_o(t_3-t_2))$	$\sin^{-1}(J_{\rm in})$
$IV:[T_3-T_4]$	S_{1B}, S_{2A}	$-I_{\rm in}$	$\frac{-I_{\rm in}}{C}(t_4-t_3)+V_o\cos(\omega_o(t_3-t_2))$	$\frac{1}{J_{\rm in}}\left(1+\sqrt{1-J_{\rm in}^2}\right)$
$V:[T_4-T_5]$	$S_{1B}, S_{2A}, D_{1B}, D_{2A}$	$-I_{\rm in}$	$-V_o$	–

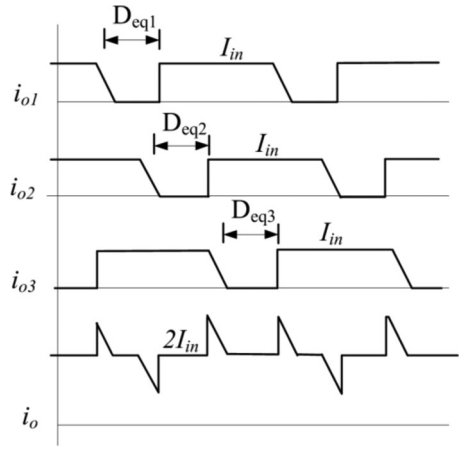

Fig. 5. Waveforms of interleaved converter operation.

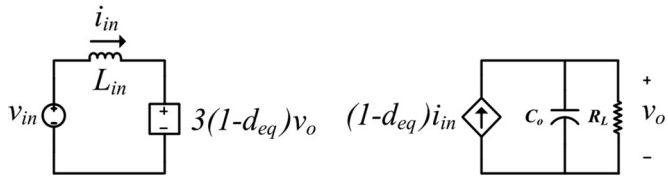

Fig. 6. Large-signal model of interleaved three-phase converter.

controlled by adjusting the value of phase shift between gate signals of the upper and lower leg switches. In other words, the converter can be simplified as a basic boost converter where the value of phase shift is equal to equivalent duty cycle. Fig. 5 shows waveforms of all the three modules and the total output currents of interleaved converter. In fact the total output current of interleaved converter tends to be a constant dc current because of phase shift of gate signals of converter modules. Output current ripple will depend on equivalent duty cycle of the converter modules and the number of modules. For the proposed three-phase converter, equivalent duty cycle of $2/3$ would give ripple-free output current. In practice, output current has small ripple due to soft-switched current commutation of lower leg switches.

IV. SMALL-SIGNAL MODELING AND FAULT-TOLERANT CONTROL

The equivalent boost circuit model proposed in last section can be used to develop small-signal model of the converter. Fig. 6 shows large-signal model of three-phase interleaved converter. Applying KVL and KCL at input port and output port of the model results in the following equations:

$$v_{\rm in} = L_{\rm in}\frac{di_{\rm in}}{dt} + 3\left(1-d_{\rm eq}\right)v_o \tag{5}$$

$$\left(1-d_{\rm eq}\right)i_{\rm in} = \frac{v_o}{R_L} + C_o\frac{dv_o}{dt}. \tag{6}$$

Control to output transfer function can be found by linear perturbation of equations mentioned earlier and then using Laplace transform equation, see (7) shown at the bottom of the page.

This transfer function can be presented as a standard second-order system

$$G_{vd}(s) = G_{d0}\frac{\left(1-(s/\omega_z)\right)}{1+(s/Q\omega_0)+(s/\omega_0)^2} \tag{8}$$

where parameters are defined as

$$G_{d0} = \frac{1}{1-D_{\rm eq}} \tag{9}$$

$$\omega_0 = \frac{1-D_{\rm eq}}{\sqrt{L_{\rm in}C_o/3}} \tag{10}$$

$$Q = (1-D_{\rm eq})R_L\sqrt{\frac{3C_o}{L_{\rm in}}} \tag{11}$$

$$\omega_z = \frac{3\left(1-D_{\rm eq}\right)^2 R_L}{L_{\rm in}}. \tag{12}$$

This model can be used to design proportional–integral (PI) compensators for output voltage regulation. Simplified control block diagram for the purposed compensator is depicted in

$$G_{vd}(s) = \frac{v_o(s)}{d_{\rm eq}(s)} = \frac{\left(V_o/(1-D_{\rm eq})\right)\left[1-(L_{\rm in}/(3(1-D_{eq})^2R_L))s\right]}{1+\left((L_{\rm in}/(3(1-D_{\rm eq})^2R_L))\right)s+(L_{\rm in}C_o/(3(1-D_{\rm eq})^2))\,s^2} \tag{7}$$

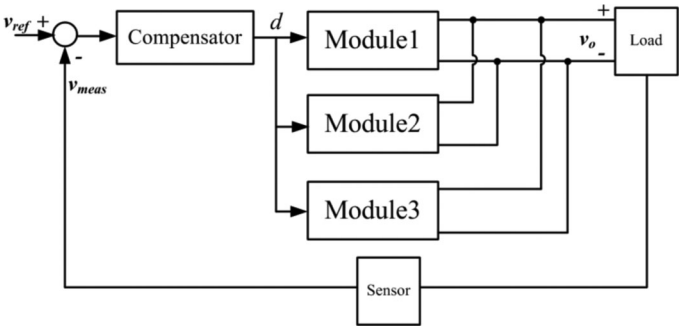

Fig. 7. Closed-loop control block diagram for three-phase converter.

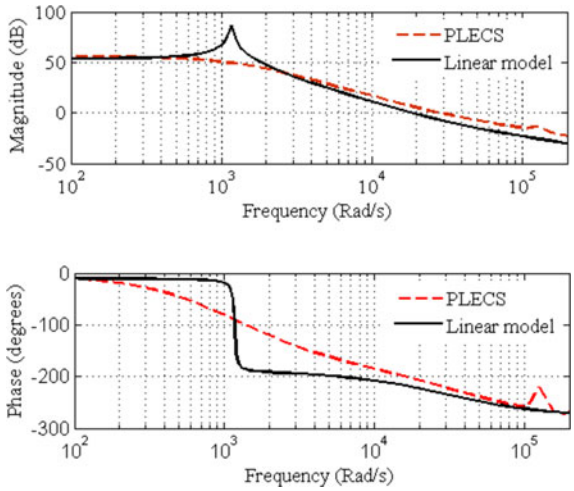

Fig. 8. Comparison of linear model Bode plot with data from PLECS switching circuit.

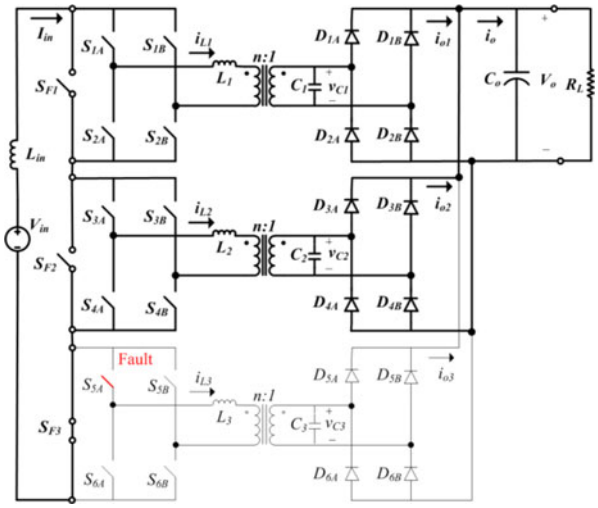

Fig. 9. Interleaved three-phase ZCS dc–dc converter.

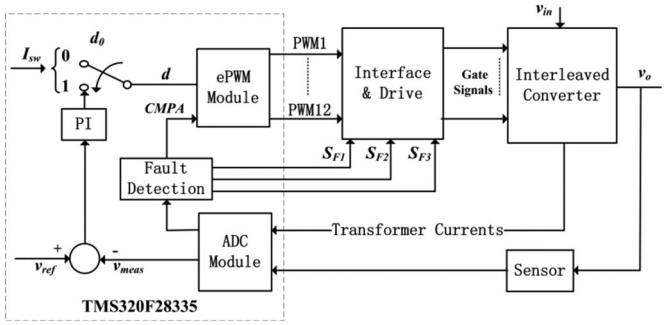

Fig. 10. Control implementation on TMS320F28335 microcontroller.

TABLE II
LABORATORY PROTOTYPE SPECIFICATION

Item	Value
Switching frequency	20 kHz
Nominal load power	3 kW
Nominal input voltage	300 V
Nominal output voltage	150 V

TABLE III
SELECTED COMPONENTS OF LABORATORY PROTOTYPE

Component	Part No./Description
Primary switches	IXGP30N120B3, High-Speed Low-Vsat PT IGBT 1200 V, 30 A with series connected C4D15120A-ND, silicon carbide Schottky diode 1200 V, 20 A
Secondary diodes	C4D15120A-ND, silicon carbide Schottky diode 1200 V, 20 A
AC capacitors	$2 * 100\text{nF}$ SMD ceramic capacitors
DC capacitors	$2 * 470\mu\text{F}$ aluminum electrolyte capacitors
Input dc inductor	1.08mH with Toroidal Ferrite Core and 108 turns of AWG 12 wire
Microcontroller	Texas Instrument TMS320F28335 DSP
IGBT driver	HCPL-3120, Avago Technologies 2.5 A Optocoupler IGBT driver
Voltage sensor	LEM LV-20 Hall effect sensor
Current sensor	ACS712ELCTR-20A-T
Transformer	1:1 turns ratio

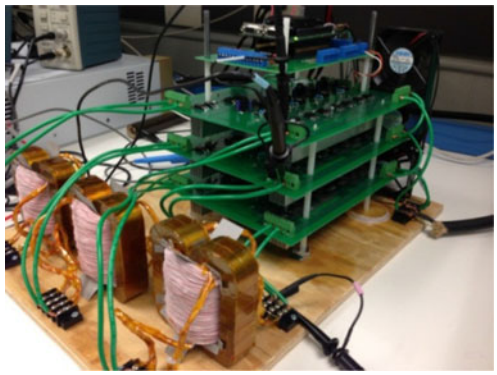

Fig. 11. Prototype of three-phase ZCS dc–dc converter.

Fig. 7. In order to validate proposed linear model, bode plot of the linear model is compared with small-signal perturbation analysis results on switching circuit obtained from PLECS. Based on comparison of linear model and switching circuit plots shown in Fig. 8, one can see that proposed linear model closely follow switching circuit model and, therefore, can be used for small-signal analysis and controller design.

Reliability and fault tolerance are essential for subsea power system. Proposed modular design is basically well suited for

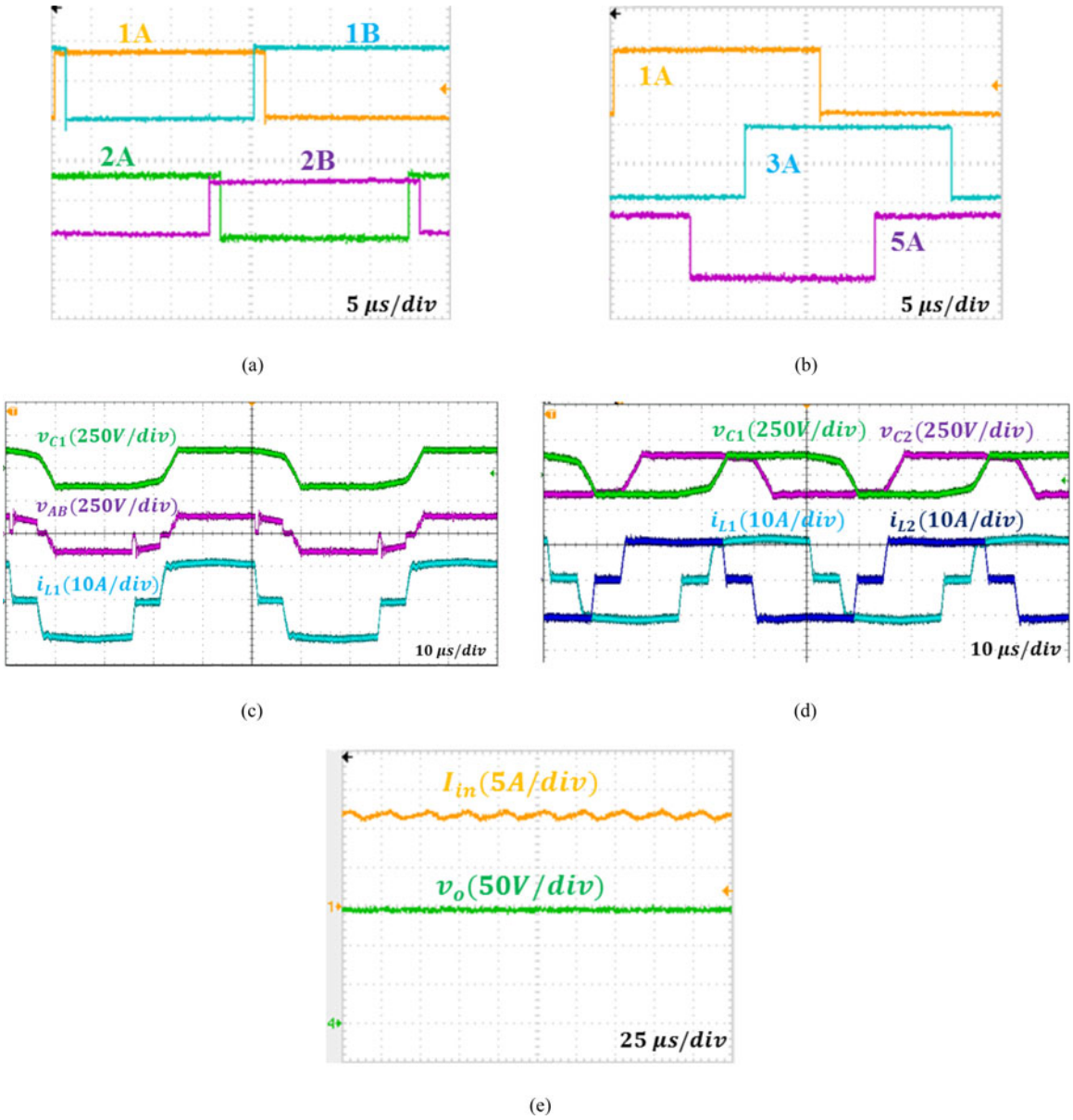

Fig. 12. Experimental steady-state test results: (a) and (b) gate signals of the converter, (c) transformer waveforms for one module of the three-phase converter, from top to bottom: secondary voltage, primary voltage, and primary current, (d) primary current (ac inductor current) and secondary voltage (ac capacitor voltage) of two phases of the three-phase converter, and (e) input current and output voltage of the three-phase converter.

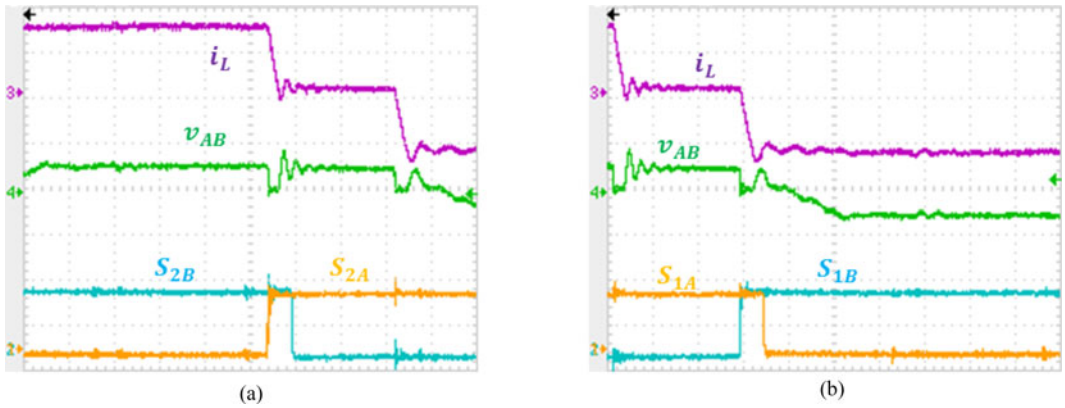

Fig. 13. ZCS of primary switches: (a) turn off of S_{2B} and (b) turn off of S_{1A}.

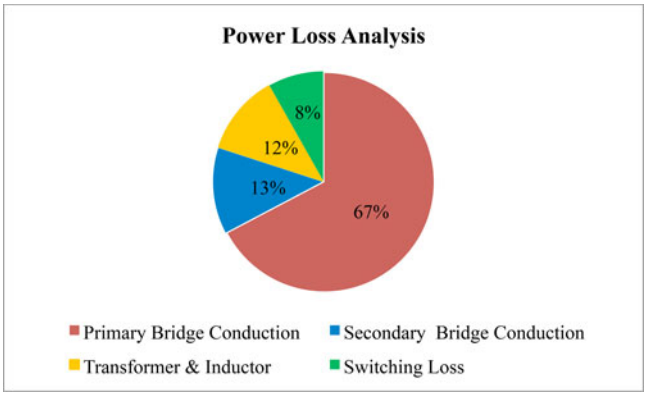

Fig. 14. Power loss analysis of the converter.

high reliability, but proper fault detection and diagnosis techniques are required in order to take advantage of system modular design. Fig. 9 shows three-phase dc–dc converter with additional bypass switches S_{F1}, S_{F2}, S_{F3} at the input of each full-bridge module. Once a fault is detected in one module, its corresponding bypass switch will close and the faulty bridge will be inactive.

For fault detection and diagnosis, it is assumed that converter is operating in continuous conduction mode (CCM) and input current is almost constant. Under normal operation, current waveform of the bridge switches are square wave pulses with 50% duty ratio (similar to gate pulse of the corresponding switch). Fault detection is carried out by sensing currents of full-bridge switches with a sampling frequency well above switching frequency and then estimation of the current pulse duty ratio. If any fault, open-circuit or short-circuit, occurs in a converter module, current pulse duty ratio will no more be 50%. At this situation, fault flag corresponding to the fault module is set and bypass switch is closed at the start of next fault detection period. Fig. 10 shows control architecture of the converter implemented on TMS320F28335 microcontroller.

V. Experimental Test Results

A scaled-down laboratory prototype of the proposed three-phase converter is implemented and experimental tests are carried out to verify the design. Table II shows specification of the prototype. Switching frequency of the converter is selected to be 20 kHz. Output voltage and power of the converter are selected to be 150 V and 3 kW, respectively. With the given load specification, a nominal input voltage of truly scaled-down converter would be 300 V. Table III shows selected components for prototype implementation. For primary bridge switches, high-speed IGBTs are used in series connection with silicon carbide Schottky diodes to provide required reverse blocking capability. The same Schottky diodes are used for secondary bridge. For resonant capacitors connected in parallel with transformer secondary, two 100 nF ceramic capacitors are used. Output capacitor of the converter is two 470 μF electrolytic capacitors. Converter control is built on TMS320F28335 microcontroller from Texas Instruments. PWM gate signals are generated using the microcontroller and are connected to IGBT gates through open-collector buffers and HCPL-3120 optocoupler. Output voltage and switch currents are sensed using LEM LV-20 and ACS712ELCTR-20A-T Hall Effect sensors, respectively. Leakage inductance of the transformer is used as required resonant inductor to achieve soft switching. Two sets of shell-type Metglas C-cores with high-permeability amorphous alloy and saturation flux density of 1.56 T are used as transformer core. Five parallel branches with 44 turns of MWS 60/36 SP-NSN155 Litz wire are used for both primary and secondary. Fish paper and Kapton tape are used for core to winding insulation and primary to secondary insulation. Input dc inductor is implemented using C0–58907A2 high-flux Toroidal Ferrite core and 108 turns of MWS HPN 155 AWG 12 wires for winding. *LCR* measurement shows 1.08 mH inductance and 48 mΩ of resistance. Fig. 11 shows picture of the implemented converter that is composed of three stacked boards, three single-phase transformers, and a digital controlled mounted on the top of the power boards.

Experimental test results are displayed in Figs. 12–16. Gate signal waveforms for phase 1 are shown in Fig. 12(a). It can be seen that gate signals of upper leg switches are complementary and gate switches of lower leg phase-shifted with respect to upper leg. Gate signal waveforms for switch *A* of each phase are shown in Fig. 12(b). Phase shift between three-phase gate signals is adjusted to ensure ripple-free output current. Fig. 12(c) shows waveforms of one of the single-phase transformers. Primary voltage is equal to zero two times over each switching cycle—first, during the overlap time of upper leg switches, and the second time during the overlap time of lower leg switches. Oscillations of the primary voltage after the overlap interval are important as they also represent voltage stress of the primary full-bridge switches. As it can be seen, peak of the ac voltage at transformer primary (peak of the voltage stress of the primary switch) is just slightly higher than the output dc voltage. Voltage waveform at the transformer secondary is of more smooth trapezoidal shape. Transformer current has a zero state in addition to positive and negative input currents. Zero current of transformer occurs during charge period of input boost inductor when both switches of one leg are closed. Peak transformer current and voltage are limited to input current and output voltage of the converter, respectively. Fig. 12(d) shows waveforms of primary current and secondary voltage of transformer for two phases of the converter. It can be seen that waveforms are 120° phase shifted like a three-phase balanced system. The input dc current and the output voltage of the converter are shown in Fig. 12(e). The dc value of the input current is 11.7 A, and the dc value of the output voltage is 150 V.

Fig. 13 shows ZCS of primary switches for an upper leg switch and a lower leg switch. Transformer primary current i_L and primary voltage v_{AB} are shown together with gate signal of IGBTs. ZCS of S_{2B} is depicted in Fig. 13(a). During S_{2B}/S_{2A} transition, S_{1A} is on and S_{2A} is turned on in advance of S_{2B} turn off. Therefore, primary current goes linearly from positive input current value to zero making ZCS possible. Fig. 13(b) shows the ZCS operation of upper switch leg where S_{1A} has soft turn off. In this case, S_{1B} is turned on and inductor current will increase

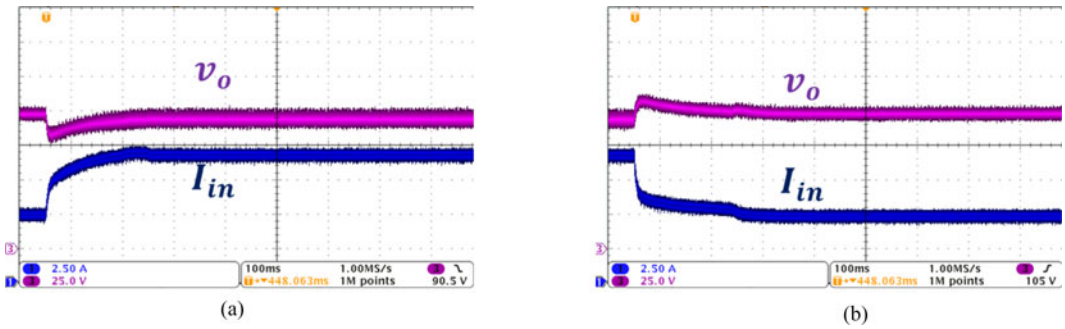

Fig. 15. Dynamic response of input current and output voltage of the three-phase converter for load change (a) from 20 to 10 Ω and (b) from 10 to 20 Ω.

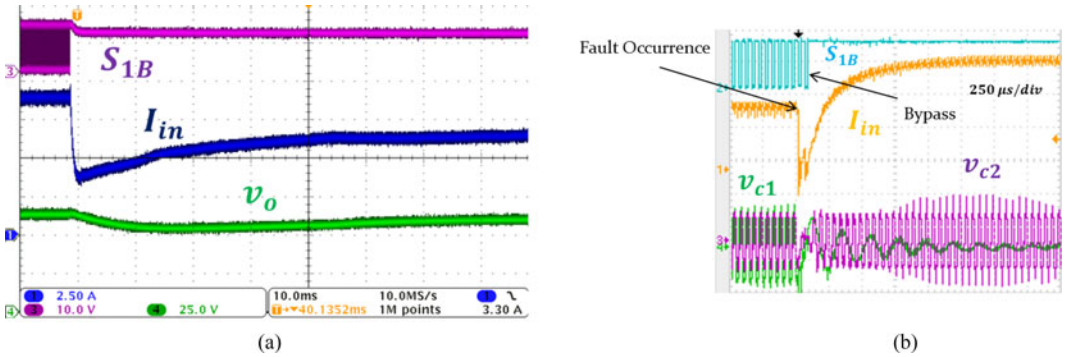

Fig. 16. (a) Input current, output voltage, and gate signal during a fault transient, (b) input current, transformer secondary voltage, and gate signal during a fault transient.

from zero to the input current values through a second-order resonant behavior. Fig. 15 shows power loss analysis of the converter while operating it with 10 A input current. Measured efficiency is about 90%. It can be seen from power loss chart that losses are dominated by primary full-bridge conduction losses. This is due to high conduction voltage of primary switches and series connection of IGBT and diode. In fact, reverse-blocking IGBTs can be used to reduce voltage drop and increase efficiency of the converter.

Fig. 15 shows results of dynamic response of the converter for a load change from 10 to 20 Ω and vice versa. The reference value of output voltage is 100 V. It can be seen that output voltage follows its reference value in spite of large change in load current with a fast dynamic response.

Test results for analysis of fault tolerance in converter are displayed in Fig. 16. It is assumed that open-circuit faults occur in one phase of the converter and that the proposed fault-tolerant control is utilized to bypass the faulty phase and continue converter operation using healthy phases of the converter. Fig. 16(a) shows fault-tolerant operation under open-circuit of switch S_{1A}. Gate signal of S_{1B}, input current $I_{\rm in}$, and output voltage v_o show proper operation of the converter under fault condition. However, dynamic response of the control system is slow. Thus, based on fault information, a feedforward approach is used to update phase shift and provide fast and smooth transient response, as shown in Fig. 16(b), for another fault-transient experiment. Gate signalS_{1B}, input current, and transformer secondary (resonant capacitor) voltages are shown in Fig. 16(b). Fault protection is activated within two switching cycle. Faulty transformer voltage declines to zero gradually, and healthy converter module keeps working to supply power to load.

VI. Conclusion

A multiphase current-fed dc–dc converter was proposed for receiving-end power conversion system in modular stacked subsea power distribution system. High-frequency isolated modular design of the proposed system architecture offers high power density and reliability. Soft switching is utilized to limit switching losses and electromagnetic interferences. A simple yet efficient model is proposed to analyze the converter operation in steady state and transients. Fault detection and fault-tolerant control strategies are developed to ensure operation of the system even under failure of one phase. Experimental test results on a scaled-down prototype confirm proposed system analysis and design.

References

[1] H. Fan and H. Li, "High-frequency transformer isolated bidirectional dc-dc converter modules with high efficiency over wide load range for 20 kva solid-state transformer," *IEEE Trans. Power Electron.*, vol. 26, no. 12, pp. 3599–3608, Dec. 2011.

[2] S. Inoue and H. Akagi, "A bidirectional isolated dc-dc converter as a core circuit of the next-generation medium-voltage power conversion system," *IEEE Trans. Power Electron.*, vol. 22, no. 2, pp. 535–542, Mar. 2007.

[3] B. Zhao, Q. Yu, and W. Sun, "Extended-phase-shift control of isolated bidirectional dc–dc converter for power distribution in microgrid," *IEEE Trans. Power Electron.*, vol. 27, pp. 4667–4680, Nov. 2012.

[4] G. Ortiz, J. Biela, D. Bortis, and J. Kolar, "1 megawatt, 20 kHz, isolated, bidirectional 12 kV to 1.2 kV dc-dc converter for renewable energy applications," in *2010 Int. Proc. Power Electron. Conf.*, 2010, pp. 3212–3219.
[5] H. R. E. Larico and I. Barbi, "Three-phase push–pull DC–DC converter: Analysis, design, and experimentation," *IEEE Trans. Ind. Electron.*, vol. 59, no. 12, pp. 4629–4636, Dec. 2012.
[6] D. Vinnikov and I. Roasto, "Quasi-Z-source-based isolated DC/DC converters for distributed power generation," *IEEE Trans. Ind. Electron.*, vol. 58, no. 1, pp. 192–201, Jan. 2011.
[7] S. Moisseev, K. Soshin, and M. Nakaoka, "Tapped-inductor filter assisted soft-switching PWM DC–DC power converter," *IEEE Trans. Aerosp. Electron. Syst.*, vol. 41, no. 1, pp. 174–180, Jan. 2005.
[8] A. K. Rathore, A. K S. Bhat, and R. Oruganti, "Analysis, design and experimental results of wide range ZVS active-clamped L-L type current-fed DC/DC converter for fuel cells to utility interface," *IEEE Trans. Ind. Electron.*, vol. 59, no. 1, pp. 473–485, Jan. 2012.
[9] L. Wuhua and H. Xiangning, "A family of isolated interleaved boost and buck converters with winding-cross-coupled inductors," *IEEE Trans. Power Electron.*, vol. 23, no. 6, pp. 3164–3173, Nov. 2008.
[10] M. Jain, M. Daniele, and P. K. Jain, "A bidirectional DC–DC converter topology for low power application," *IEEE Trans. Power Electron.*, vol. 15, no. 4, pp. 595–606, Jul. 2000.
[11] U. R. Prasanna, A. K. Rathore, and S. K. Mazumder, "Novel zero-current-switching current-fed half-bridge isolated DC/DC converter for fuel-cell-based applications," *IEEE Trans. Ind. Appl.*, vol. 49, no. 4, pp. 1658–1668, Jul.–Aug. 2013.
[12] U. R. Prasanna and A. K. Rathore, "Current-fed interleaved phase-modulated single-phase unfolding inverter: Analysis, design, and experimental results," *IEEE Trans. Ind. Electron.*, vol. 61, no. 1, pp. 310–319, Jan. 2014.
[13] M. Nymand and M. A E. Andersen, "High-efficiency isolated boost DC–DC converter for high-power low-voltage fuel-cell applications," *IEEE Trans. Ind. Electron.*, vol. 57, no. 2, pp. 505–514, Feb. 2010.
[14] C. Honnyong, D. Rongjun, T. Qingsong, and F. Z. Peng, "Design and development of high-power DC–DC converter for metro vehicle system," *IEEE Trans. Ind. Appl.*, vol. 44, no. 6, pp. 1795–1804, Nov.–Dec. 2008.
[15] H. Rongjun and S. K. Mazumder, "A soft switching scheme for multiphase DC/pulsating-DC converter for three-phase high-frequency-link pulsewidth modulation (PWM) inverter," *IEEE Trans. Power Electron.*, vol. 25, no. 7, pp. 1761–1774, Jul. 2010.
[16] J. A. Abu-Qahouq, H. Mao, H. Zhou, and I. Batarseh, "DC–DC converter with interleaved current doublers and parallel connected transformers-scheme," *IET Power Electron.*, vol. 1, pp. 27–37, Mar. 2008.
[17] Z. Al-Haiki and A. Shaikh-Nasser, "Power transmission to distant offshore facilities," *IEEE Trans. Ind. Appl.*, vol. 47, no. 3, pp. 1180–1183, May-Jun. 2011.
[18] S. Schroder, P. Tenca, T. Geyer, P. Soldi, L. Garces, R. Zhang, T. Toma, and P. Bordignon, "Modular high-power shunt-interleaved drive system: A realization up to 35 mw for oil and gas applications," *IEEE Trans. Ind. Appl.*, vol. 46, no. 2, pp. 821–830, Mar.–Apr. 2010.
[19] M. Popat, B. Wu, and N. R. Zargari, "A novel decoupled interconnecting method for current-source converter-based offshore wind farms," *IEEE Trans. Power Electron.*, vol. 27, no. 10, pp. 4224–4233, Oct. 2012.
[20] Y. Li, Z. Zhang, C. Rehtanz, L. Luo, S. Ruberg, and F. Liu, "Study on steady- and transient-state characteristics of a new hvdc transmission system based on an inductive filtering method," *IEEE Trans. Power Electron.*, vol. 26, no. 7, pp. 1976–1986, Jul. 2011.
[21] N. Flourentzou, V. Agelidis, and G. Demetriades, "VSC-based HVDC power transmission systems: An overview," *IEEE Trans. Power Electron.*, vol. 24, no. 3, pp. 592–602, Mar. 2009.
[22] A. Prasai, J.-S. Yim, D. Divan, A. Bendre, and S.-K. Sul, "A new architecture for offshore wind farms," *IEEE Trans. Power Electron.*, vol. 23, no. 3, pp. 1198–1204, May 2008.
[23] J. Song-Manguelle, R. Datta, M. Harfman Todorovic, R. Gupta, D. Zhang, S. Chi, L. Garces, and R. Lai, "A modular stacked dc transmission and distribution system for long distance subsea applications," in *Proc. IEEE Energy Convers. Congress Expo.*, 2012, pp. 4437–4444.
[24] A. Mohammadpour, L. Parsa, M. H. Todorovic, L. Rixin, and R. Datta, "Interleaved multi-phase ZCS isolated DC–DC converter for sub-sea power distribution," in *Proc. Annu. Conf. IEEE Ind. Electron. Soc.*, Nov. 10–13, 2013, pp. 924–929.
[25] C. Iannello, S. Luo, and I. Batarseh, "Full bridge ZCS PWM converter for high-voltage high-power applications," *IEEE Trans. Aerosp. Electron. Syst.*, vol. 38, no. 2, pp. 515–526, Apr. 2002.

Ali Mohammadpour received the B.S. degree from the University of Tabriz, Tabriz, Iran, in 2007, the M.S. degree from Sharif University of Technology, Tehran, Iran, in 2009, and the Ph.D. degree from Rensselaer Polytechnic Institute, Troy, NY, USA, in 2014, all in electrical engineering.

From 2008 to 2010, he was a Power Electronics Engineer in the industry. He is currently a Power Electronics Research Engineer at Bose Corporation, Framingham, MA, USA. His current research interests include multiphase power electronic systems and converters.

Leila Parsa (S'00–M'05–SM'10) received the Ph.D. degree in electrical engineering from Texas A&M University, College Station, TX, USA.

In 2005, she joined the Department of Electrical, Computer, and Systems Engineering, Rensselaer Polytechnic Institute, Troy, NY, USA, where she is currently an Associate Professor. Her current research interests include design, analysis, and control of electromechanical energy converters and power electronics converters for various applications.

Dr. Parsa was the recipient of the 2010 RPI School of Engineering Research Excellence Award, the 2009 Office of Naval Research Young Investigator Award, the 2007 IEEE Industry Applications Society Outstanding Young Member Award, and the 2006 IEEE Industry Applications Society Transactions Paper Award.

Maja Harfman Todorovic, photograph and biography not available at the time of publication.

Rixin Lai, photograph and biography not available at the time of publication.

Rajib Datta, photograph and biography not available at the time of publication.

Luis Garces, photograph and biography not available at the time of publication.